UDC 669 . 184 . 244 . 66 : 539 . 072

Technical Report

Behavior of Top-blowing Lance Jets in BOF

Ken-ichiro NAITO*
Akihide KAIZAWA
Itsuro KITAGAWA
Naoto SASAKI
Norifumi ASAHARA
Yuji OGAWA
Takeo INOMOTO
Michitaka MATSUO

Abstract

While the role of top-blown jet as a source of stirring energy has decreased with the introduction of the combined blowing technology to BOF, the flexibility of lance design and its operation has considerably increased. Besides, with the expanding application of hot metal pretreatment using BOF, the demands for the optimization of top-blown jet has been increasing. Meanwhile, computational fluid dynamics (CFD) has become popular in steelmaking area owing to the recent advancement of computational capacity and has enabled the numerical simulation of complicated phenomena. Nippon Steel Corporation, through experiments and CFD analysis, has been promoting to elucidate the phenomena related to top-blown jet such as incorrect expansion, interference and coalescence of jets, interaction with liquid bath and behavior in the combustion field and the quantitative estimation is becoming possible. Based on the obtained knowledge, dimension of toplance and its operating condition are designed and applied to the commercial production such as high-speed blowing.

1. Introduction

The top-blowing lance jet of a converter works as the source of feeding oxygen and energy for stirring molten iron. Major in-furnace phenomena of a converter that involve the top-blowing lance jet are formation of a cavity as a result of physical interaction between a jet and molten iron, stirring of molten iron, generation of spitting and dust, and postcombustion of CO gas generated by decarburization and reaction with oxygen. Formerly, to optimize converter operation and control the phenomena stated above, various devices and improvements have been made and applied to the design and operation of top-blowing lances. Examples of these include the employment of Laval nozzles for a top-blowing lance capable of converting pressure energy to jet kinetic energy with high efficiency in order to promote stirring of molten iron, and the general use of a multi-hole lance that enables high-speed oxygen feeding while suppressing generation of spitting and dust by dispersing the jet from a top-blowing lance.[1)]

Since the 1980s, with the introduction of combined blowing type converters, the role of top-blowing lance jets as the source of energy for stirring molten iron declined and flexibility in design and operation has been enhanced significantly. On the other hand, since the later half of the 1990s, Nippon Steel Corporation has promoted the expansion of the application of converter type pretreatment processes such as the multi-refining converter (MURC) process.[2, 3)] For MURC, demands increased for further optimization of the top-blowing lance jet, to realize compatible blowing of dephosphorization and decarbulization with a single lance, and high-speed blowing, to suppress deterioration of productivity caused by additional processes such as intermediate slag discharge and slag solidification.

On the other hand, along with the advancement of computational capacity in recent years, computational fluid dynamics (CFD) analysis technology has come to be used more widely in the field of steelmaking, and although once considered to be difficult, simulation of complicated phenomena involving compressible fluid, multi-phases, and reactions has become possible.

This article describes an experiment for the measurement of jet behavior at ordinary temperature, a combustion experiment, and CFD simulation, all of which Nippon Steel Corporation has conducted as a part of elucidating the phenomena related to top-blowing lance jets.

* Chief Researcher, Steelmaking R&D Div., Process Technology Center
20-1 Shintomi, Futtsu, Chiba 293-8511

2. Behavior of a Single-hole Nozzle Jet [4-6)]

2.1 Outline

As described above, a Laval type nozzle (convergent–divergent nozzle), capable of efficiently converting pressure energy to kinetic energy of a jet, is generally used for the top-blowing lance of a converter. The dimensions of a Laval nozzle determines the correct Mach number, correct pressure, and correct flow rate, and normally, the nozzle is operated under its correct condition (correct expansion) or in its neighborhood. On the other hand, it is known that the operation in the region outside correct expansion generates shock and expansion waves, causing greater loss in jet energy. This is termed as incorrect expansion.

This chapter describes the experiment and the CFD analysis concerning the behavior of a single-hole nozzle jet, including the case of incorrect expansion.

2.2 Experiment and analysis method

Five different single-hole nozzles having identical throat diameters and different outlet diameters for each nozzle were used under ordinary ambient condition, and the nozzle inlet pressure (flow rate) was changed and the velocity distribution of the jet was measured by a Pitot's tube.

Because the minimum detectable limit of the measurement equipment was 5.7 m/s, the radius of the region wherein the fluid velocity is above the minimum limit was taken as the jet radius.

Furthermore, the two-dimensional axisymmetrical model of the commercially available CFD code, FLUENT,[7)] was used for CFD analysis, where the inflow mass condition and the outflow pressure condition were used as the boundary conditions of the entry and outlet sides, respectively. The physical property of air was used for the gaseous phase, wherein compressibility of air was considered.

2.3 Results and discussion

2.3.1 Behavior under incorrect expansion

Fig. 1 shows an example of the measured results for the velocity of a jet from a single-hole nozzle at the position $x/d_t = 20.5$, a position made dimensionless by dividing x, the distance from the nozzle outlet, by d_t, the nozzle throat diameter.

At this position, the velocity was measured for two types of nozzles: one having a P_{0p} of 0.186 MPa (straight nozzle) and another having a P_{0p} of 0.392 MPa (Laval nozzle), wherein P_{0p} is the correct nozzle inlet pressure determined by the ratio of the throat diameter to the nozzle outlet diameter. Comparison of the change in the central axial jet velocity (in Mach number) vs. the change in the operating pressure P_0 at the nozzle inlet is shown.

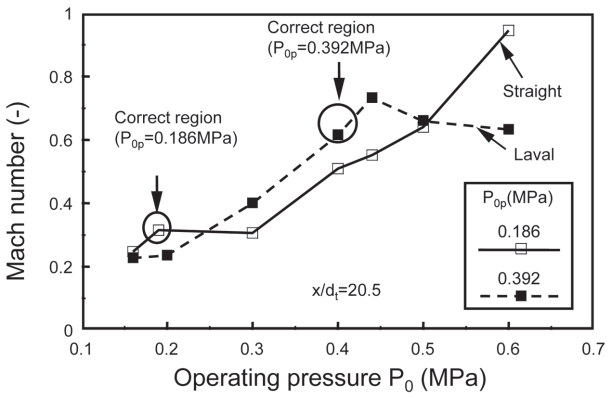

Fig. 1 Relation between operating pressure and central axial jet velocity (Mach number)

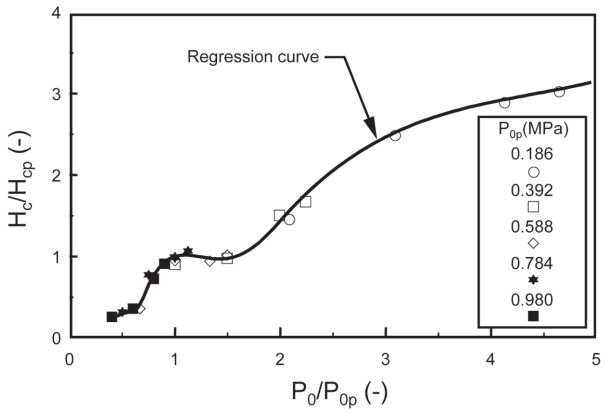

Fig. 2 Relation between P_0/P_{0p} and H_c/H_{cp}

In both cases, the following phenomena were observed: ① Velocity increases once as operating pressure increases. ② However, there is a region where velocity does not increase after it reaches a peak at and near the correct pressure. ③ The velocity starts increasing again thereafter. In the region where velocity does not increase despite increase in operating pressure, it is considered that the loss in energy due to incorrect expansion offsets the increase in pressure energy.

Then, in **Fig. 2**, defining the ratio of the operating pressure at the nozzle inlet P_0 to the correct pressure P_{0p} (P_0/P_{0p}) as degree of incorrectness, the central axial jet velocity is shown with respect to the order of P_0/P_{0p}. Because it is known that the central axial jet velocity attenuates in inverse proportion to the distance from the nozzle exit, when the position where the jet velocity becomes equal to sound velocity (Mach number: 1) is expressed as H_c (jet core length), the jet velocity (Mach number) at an arbitrary position on the central axis is expressed by equation (1). Then, in Fig. 2, the axis of ordinate H_c/H_{cp}, the ratio of the jet core length to the jet core length in a state of correct expansion (H_{cp}), represents central axial jet velocity. Furthermore, the jet core length under a state of correct expansion is expressed by equation (2), the details of which are omitted here.

$$M = H_c / x \quad (1)$$

$$H_{cp} = M_{0p} \cdot (5.88 + 1.54 M_{0p}^2) \cdot d_t \quad (2)$$

where H_{cp} is the jet core length in a state of correct expansion and M_{0p} is the Mach number at discharging from the nozzle in a state of correct expansion.

As shown in Fig. 2, the central axial jet velocity of each nozzle in a state of incorrect expansion can be shown approximately with a unitary curve, and thereby, estimation of the jet velocity in a state of incorrect expansion is made possible. Therefore, by applying this result and by utilizing an incorrect expansion positively, a softly blown jet can be realized.

2.3.2 CFD analysis

Through a comparison between the measured and CFD simulated results computed by various turbulent flow models employed in FLUENT and from the viewpoints of computation accuracy and computation cost, a standard k-ε model was finally selected for analysis of the central axial jet velocity. This model has been used in analysis since then.

Comparisons between the CFD simulated and measured central axial jet velocity are shown in **Fig. 3**. The velocity attenuates in inverse proportion to the distance from the nozzle tip. Although the

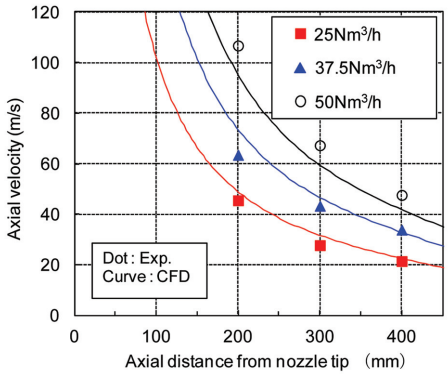

Fig. 3 Comparison between CFD simulated and measured central axial jet velocity

trend of the calculated result approximately agrees with that of the measured result, change in difference is between CFD results and experiments when flow rate increases. In the experiment, a nozzle with a correct flow rate of 52 Nm^3/h in the state of correct expansion was used. Therefore, a flow rate of 50 Nm^3/h lies almost in the correct expansion region, whereas flow rates of 25.0 Nm^3/h and 37.5 Nm^3/h are in the region of overexpansion. Comparison of the calculated and measured results reveals that the calculated result is lower than the measured result in the state of correct expansion, while the calculated result is higher in the state of overexpansion. This means that the behavior under a state of incorrect expansion has not been well reproduced by the CFD simulation, leaving a subject for further examination.

Further, the jet radius will be discussed in 3.3.

3. Behavior of a Multi-hole Nozzle Jet [4-6)]

3.1 Outline

As described above, for the top-blowing lance of a converter, multi-hole nozzles are generally used that enable high-speed oxygen feeding while suppressing the generation of spitting and dust by dispersing the jet. However, the soft-blowing effect, as mentioned above, cannot be obtained when jet interference and coalescence take place.

In this chapter, the experiment and CFD simulation of the behavior of a multi-hole nozzle jet are described.

3.2 Experiment and analysis method

The experimental method is the same as that in 2.2. The specification of the multi-hole nozzles is shown in **Table 1**. The total area of each throat area and the ratio of the throat diameter to the outlet diameter are the same for all nozzles.

Furthermore, as for the evaluation of multi-hole nozzle jet dispersion, as shown by the schematic illustration in **Fig. 4**, the jet radius of a nozzle is defined as the radius of the circumscribing circle encircling all circles of jets from their nozzle holes at their points where jet velocities are 5.7 m/s.

Table 1 Dimension of multi-hole nozzles

	Number of holes (-)	Inclined angle (deg)	Throat diameter (mm)	Outlet diameter (mm)
3 h	3	14	5.77	6.36
4 h 14 d	4	14	5.00	5.51
4 h 18 d	4	18	5.00	5.51
6 h	6	14	4.08	4.50
8 h	8	14	3.54	3.90

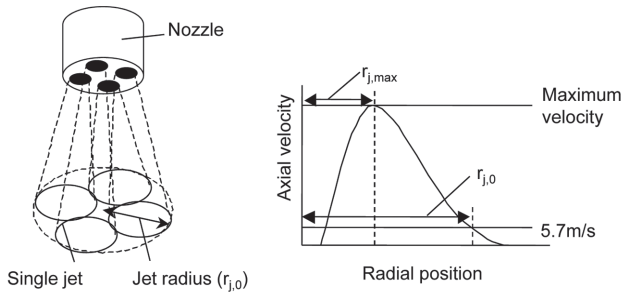

Fig. 4 Schematic illustration of jet radius

Also, as for the CFD simulation, a 3D model of FLUENT was used. As for the nozzle with "n" holes, the nozzle circle was divided in the circumferential direction into "$2n$" regions, and in a region so divided to $1/2n$, a mesh was formed for analysis, with the divided face taken as the symmetry boundary condition.

3.3 Results and discussion

An example of the measurement result for the axial velocity of a multi-hole nozzle jet is shown in **Fig. 5**. The distance from the nozzle center line in the radial direction perpendicular to the nozzle center axis is taken on the horizontal axis and the jet velocity in the axial direction is taken on the vertical axis. Jet velocity distributions of a nozzle with four holes and an inclined angle of 14° and those of a nozzle with eight holes and an inclined angle of 14° were compared. In the case of a single-hole nozzle, the smaller the nozzle diameter, the more readily a jet tends to attenuate, and therefore velocity decreases readily too. However, in the case of a multi-hole nozzle, it is found that even if holes are increased in number and the diameter of each nozzle hole is decreased accordingly, the velocity would become rather higher as attenuation of the jet is suppressed by the mutual interference and coalescence of multiple jets. In the figure, the result of CFD simulation is also shown, and the phenomenon of the above-mentioned state of interference and coalescence of jets is mostly reproduced.

Further, in **Figs. 6** and **7**, comparisons between the measured and CFD simulated results of central axial jet velocity and jet radius are shown. Since both results approximately agree regardless of the type of nozzle, it is found that the CFD analysis method is reasonable.

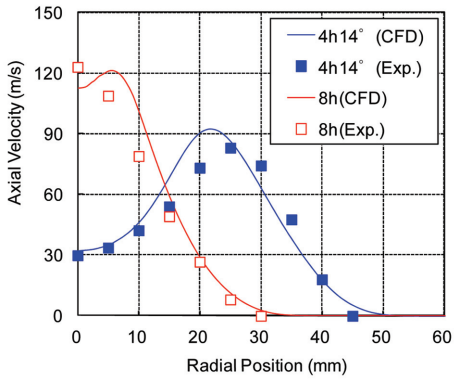

Fig. 5 Axial jet velocity of multi-hole nozzles

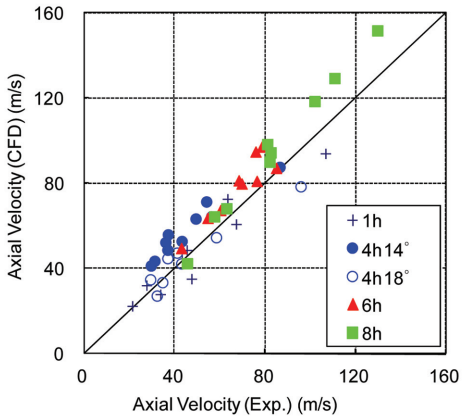

Fig. 6 Comparison between CFD simulated and measured central axial jet velocity of multi-hole nozzles

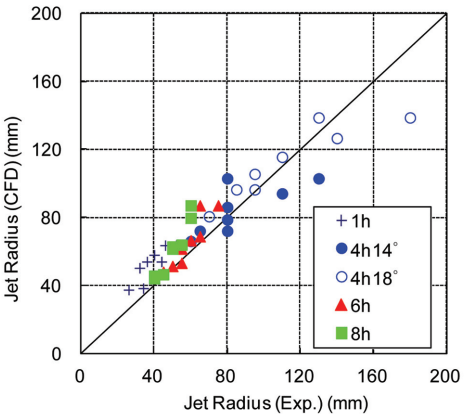

Fig. 7 Comparison between CFD simulated and measured jet radii of multi-hole nozzles

4. Interaction between a Jet and Bath [5, 6]

4.1 Outline

Physical interaction between a top-blowing lance jet and molten iron bath is a significant factor in optimizing the converter operation. Particularly, since formation of a cavity and generation of spitting are phenomena that concern refining process characteristics and generation of dust, an experiment based on a water model with single-hole nozzles was conducted in the past and the effects of top-blowing conditions were studied.[8-10] However, there are a few reports of experiments using multi-hole nozzles.[11]

This chapter describes the result of the experiment conducted to study how a cavity is formed and developed and how spitting is generated and developed concerning the interaction between a jet and bath.

4.2 Experiment and analysis method

The experiment was conducted in the following manner:

① A water model was used.
② Air was injected from top through various types of nozzles onto the surface of the water bath in a cylindrical container.
③ The situation was recorded with a video camera.
④ Cavity shape was defined (in terms of depth, diameter) on the basis of the video recording.

The relation between the result and top-blowing jet was studied. Further, as for the cavity formed by a multi-hole nozzle, the radius of the circumscribing circle was taken as cavity radius in a mannar similar to that of jet radius.

As for spitting, sampling holes were opened on the wall of the cylindrical container at a constant interval above the water bath surface and splash water drops caused by the collision of the top-blowing jet with water were sampled for the calculation of the spitting-sampling-rate per unit area at each sampling hole.

As for the CFD analysis, the volume of fluid model (VOF), a multi-phase flow model, was used and change in shape on the free surface by the effect of a gas jet was studied.

4.3 Results and discussion

4.3.1 Measurement of cavity shape with the water model

A cavity shape developed by a four-hole nozzle is shown in **Fig. 8** as an example. The cavity shape (depth, diameter, cavity angle) was defined as shown in the same figure.

As for the cavity formed by the collision of a single-hole nozzle jet, equation (3) is reported as the estimation equation for the cavity depth.[9, 12, 13]

$$M/\rho_l g h^3 = (\pi/\beta)\,(L/h)\,(1+L/h)^2 \qquad (3)$$

where M is the momentum of jet, L is the cavity depth, h is the lance height, ρ_l is the density of liquid, and g is the gravitational acceleration. β is a constant and has been reported as being 125.[12]

The measurement result for the cavity depth for each nozzle is shown in **Fig. 9**. The calculation results for nozzles with one, three, and four holes show good agreement with the measurement results, whereas for nozzles with six and eight holes, the measurement results were much greater than the calculation results. This is owing to the assumption in equation (3) that a jet from each hole is independent,

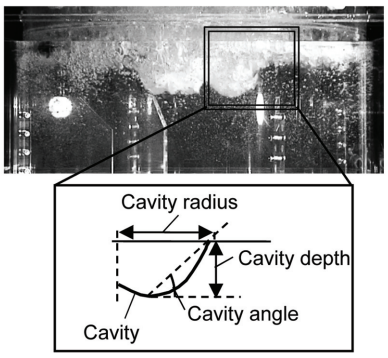

Fig. 8 Image of observed cavity

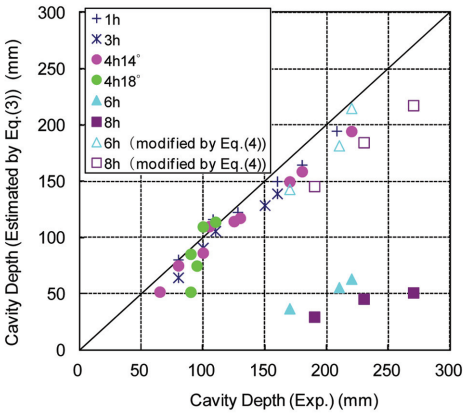

Fig. 9 Comparison between calculated and measured cavity depth

whereas for nozzles with multiple holes, the jet velocity is actually maintained at a high level owing to the interference and coalescence of jets. Then, a trial was attempted to amend the estimation equation with equation (4), assuming that the coalescence of jets from a multi-hole nozzle exists and that the cavity depth generated by a multi-hole nozzle jet is the same as the cavity depth developed by an equivalent single-hole nozzle having the same throat section area as the total throat area of the multi-hole nozzle.

$$M_{total} = nM \quad (4)$$

where M_{total} is the total momentum of a multi-hole nozzle, M is the momentum of the jet from each hole, and n is the number of holes.

By using M_{total} instead of M in equation (3), the cavity depth under the condition of coalescence of jets could be estimated as shown in Fig. 9.

However, the cavity radius tends to become larger than jet radius, and it is considered that a jet collides with the bath and reverses its direction at the bottom of a cavity, causing a force that works to push the cavity wider sideward. Then, for estimating the cavity radius (r_c), equation (5) was studied as the estimation equation:

$$r_c = r_{j,\max} + 2\,(r_{j,0} - r_{j,\max}) \quad (5)$$

where $r_{j,\max}$ is the radial position at which the velocity becomes maximum, $r_{j,0}$ is the jet radius, whose schematic illustration is shown in Fig. 4. Here, in the case of a single-hole nozzle, since $r_{j,\max} = 0$, it was assumed that the cavity radius is two times the jet radius, and in the case of a multi-hole nozzle, a similar assumption is applicable by additionally considering the center-off-ness from the jet center.

As shown in **Fig. 10**, the measurement result for the cavity radius and the result calculated by equation (5) mostly show good agreement, and therefore, it is found that the estimation of the cavity radius is possible by CFD analysis of jets.

4.3.2 Direct analysis of cavity by CFD

Concerning the cavity shape formed by a single-hole nozzle jet, an example of the result of an attempt of direct analysis by CFD is shown in **Fig. 11**. Though qualitatively, formation of a cavity on the water surface by a jet can be reproduced. However, when the measured and CFD simulated results for a cavity depth are compared, it is found that although a correlation is observed between the two, the CFD simulated results tend to be less, and therefore, quantitative estimation of the cavity depth by CFD still needs further examination.

On the other hand, the result of measurement of the cavity radius mostly showed agreement with the result of CFD simulation. The flow pattern near the cavity is shown in **Fig. 12**. From this figure, it is found that a jet flows upward as a reversing flow after reaching the cavity surface and as this flow pushes the cavity in the radial direction, a cavity with a radius larger than the jet radius is formed. In this figure also, the cavity radius is twice the jet radius; therefore, it can be said that the assumption of equation (5) is reasonable.

4.3.3 Spitting

As an example of the distribution of the spitting sampling rate in the vertical direction, the result of an experiment conducted with a three-hole nozzle at a lance height of 400 mm is shown in **Fig. 13**, and it was found that the sampling rate per unit area at a sampling height h (m), R (kg/m^2·s), can be expressed by an exponential function as

$$R = R_0 \cdot \exp(-h/h_0) \quad (6)$$

here, R_0 is the sampling rate at the sampling height $h = 0$ and is con-

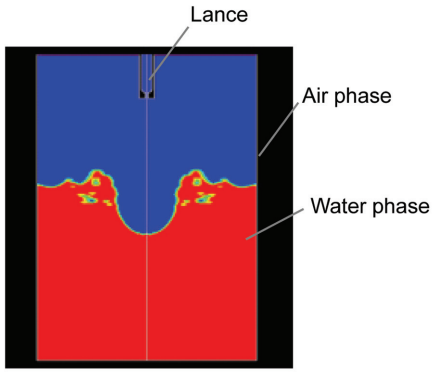

Fig. 11 CFD simulation of cavity formation

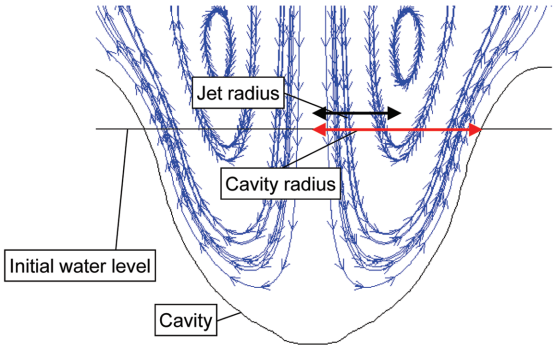

Fig. 12 Flow pattern near cavity

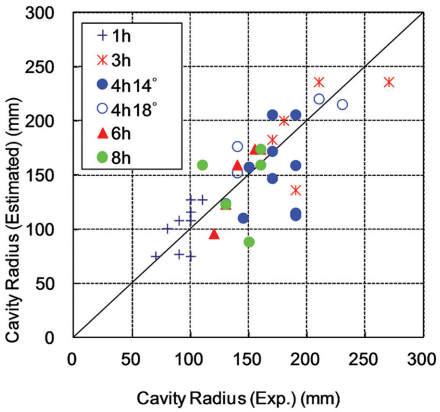

Fig. 10 Comparison between calculated and measured cavity radius

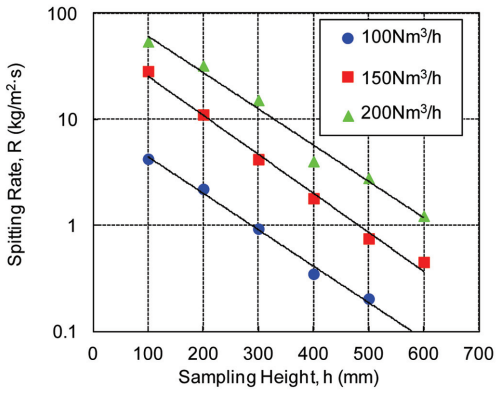

Fig. 13 Vertical direction distribution of the spitting rate

sidered to be a value representing the spitting generating rate. Furthermore, h_0 can be defined as the height at which the point sampling rate becomes R_0/e. (Here, "e" denotes the base of the natural logarithm.) Here, parameters R_0 and h_0 are fixed from the experimental result by fitting and its relations with the aforementioned jet velocity and cavity shape have been studied.

It is reported that in the case a single-hole nozzle is used, the spitting generating rate is correlated to the total momentum of the colliding jet.[10] On the other hand, in the case a multi-hole nozzle is used, as jets are not axially symmetric, the spitting scattering direction cannot be axially symmetric. Then, momentum, with due consideration paid to orientation dependency, is defined by equation (7):

$$M = \int \rho_g \cdot u(r)^2 \cdot 2\pi r \cdot dr \qquad (7)$$

where ρ_g is the density of the jet gas and $u(r)$ is the axial jet velocity at the radial position "r." For $u(r)$, the velocity distribution in the direction in which spitting was sampled was used.

The parameter R_0 obtained in the water model experiment was compared with the jet momentum calculated by equation (7) and the jet velocity distribution obtained by the CFD simulation, and a good correlation was obtained as shown in **Fig. 14**. Thereby, it was found that the spitting generating rate can be estimated by finding the velocity distribution by CFD simulation.

On the other hand, although h_0 is a parameter regarding distribution in the vertical direction, and a tendency was observed in the water model experiment in that water drops splash higher upward as the cavity becomes deeper, h_0 is considered to be related to the cavity shape. Then, h_0 was compared with the cavity angle (Refer to Fig. 8) for a single-hole nozzle, and as **Fig. 15** shows, the larger the cavity angle, the larger h_0, and a good correlation between the two was observed.

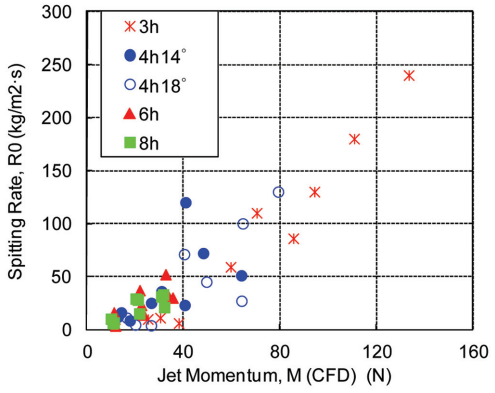

Fig. 14 Relation between the jet momentum and spitting parameter R_0

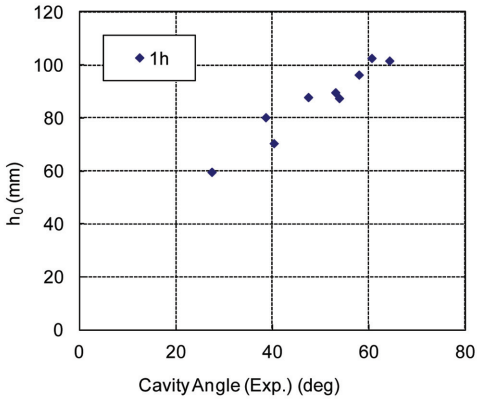

Fig. 15 Relation between the cavity angle and spitting parameter h_0

From the above-mentioned result, although it is still difficult to sufficiently reproduce the interaction between a jet and bath by direct analysis by CFD, since momentum of a colliding jet and cavity shape (depth, radius) can be estimated by CFD simulation of jet velocity distribution, it was shown that by using such parameters, it has become possible, though indirectly, to quantitatively estimate the spitting generating rate and spitting scattering height.

5. Behavior of Jet in the Combustion Field[14]

5.1 Outline

In the foregoing chapters, the behavior of a jet under the condition of room temperature without any combustion reaction has been discussed. However, inside a converter is a combustion field at high temperature, and therefore, top-blowing lance jet characteristics exert influence over the postcombustion of CO gas and the oxygen jet, and postcombustion itself also exerts influence over the jet behavior. Although research was conducted regarding the effects of the behavior of a supersonic jet under a high temperature condition without combustion[15] and top-blowing condition on postcombustion[16-18], knowledge is scarce as to the effect of gas composition change in a combusting jet.

This chapter outlines the experiment and CFD simulation about the behavior of a jet in a combustion field.

5.2 Experiment and analysis method

In addition to measuring gas concentration and temperature in a combustion experiment, an attempt was made to develop a model to reproduce by CFD the result of an experiment and to estimate the behavior of a jet.

In a combustion experiment, the behavior of CO gas combustion by an oxygen jet was studied. The gas combustion space of the experimental equipment was cylindrical and was 1,400 mm in height and had an internal diameter of 300 mm wherein

① 20 Nl/min of oxygen was fed through a 4 mm diameter single-hole nozzle of a top-blowing lance.
② 60 Nl/min of CO gas was fed through a porous plug installed at the bottom.
③ The gas was ignited by a heating resistor installed inside.
④ At predetermined points, the ambient gas temperature was measured and sampling of the gas was conducted.
⑤ Finally, the gas was analyzed.

FLUENT was used for CFD analysis, and the flow and combustion under the experimental condition were calculated, and gas concentration and temperature under a steady condition were evaluated. Calculation was performed on a 2D cylindrical coordinate. A standard k-ε model was used as the turbulent flow model, and assuming that the combustion reaction is rate-controlled by CO and O_2, an eddy dissipation model was used, wherein only the irreversible reaction of CO_2 formed from CO and O_2 was taken into consideration. Additionally, calculation was performed by changing the conditions of compressibility, radiation, and so on. The calculation result using the DO model[7] as the radiation model and taking compressibility into account showed the best agreement with the experimental result. (The DO model is a model that discretizes a spherical orientation into an azimuth φ and a zenithal angle θ, and precisely solves the orientation dependency of radiation intensity). Therefore, the condition was adopted in the calculation.

5.3 Result and discussion

5.3.1 Gas concentration distribution, temperature distribution

Fig. 16 shows the CFD-simulated gas concentration, tempera-

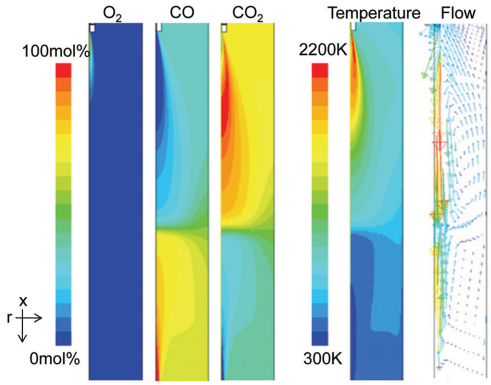

Fig. 16 Profile of gas species, temperature and flow pattern by CFD simulation

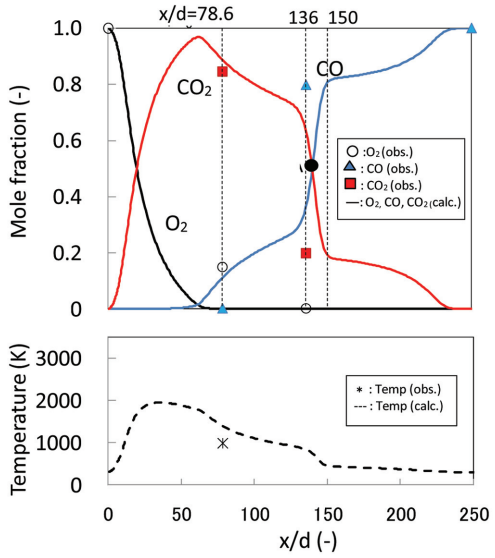

Fig. 17 Comparison between CFD simulated and measured profile of gas species and temperature on the central axis

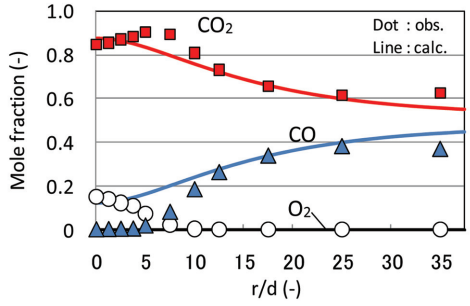

Fig. 18 Comparison between CFD simulated and measured profile of gas species in the radial direction

ture, and flow pattern. In Fig. 16, it is observed that an oxygen jet collides with CO gas and that CO_2 is formed by the combustion of CO in the neighborhood of the oxygen jet.

Further, **Figs. 17** and **18** show the measured and CFD-simulated results of respective gas concentration and temperature on the central jet axis and distribution in the radial direction. Here, x is the distance from the nozzle tip, and r is the distance in the radial direction

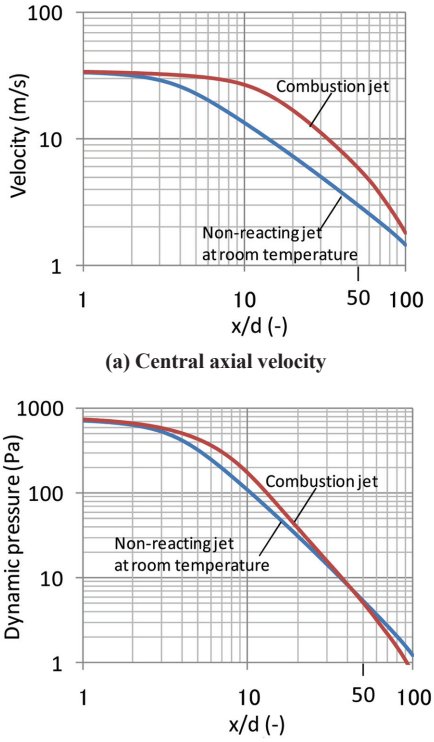

Fig. 19 Comparison between the combustion jet and non-reaction jet at room temperature

from the center axis, either of which is made dimensionless, each being divided by the nozzle internal diameter d. When the measured and CFD-simulated results are compared, although gap of a certain degree is noticed in certain areas, they agree mostly, and therefore, it is considered that a model capable of reproducing the measured result of gas concentration distribution and temperature has been established. However, regarding the oxygen concentration distribution of a top-blowing jet, the gap still remains unsolved, needing further examination.

5.3.2 Velocity, dynamic pressure, gas concentration in the combustion field

The jet characteristics (velocity, dynamic pressure, gas concentration) in a combustion field and at a nonreaction room temperature were simulated using the model shown in the above section and then compared.

In **Fig. 19**, the relation between x/d and the central axial jet velocity and the relation between x/d and the dynamic pressure are shown. In the neighborhood of $x/d = 50$ that corresponds to the bath surface in the actual production process, the combustion jet velocity becomes large, twice the jet velocity at room temperature. On the other hand, as for the dynamic pressure that is considered to influence the stirring force and spitting generation, difference between the one under combustion and the one at room temperature grows smaller, and near $x/d = 50$, they become almost the same. This is attributed to high temperature decreasing the density of the gas, and thereby, offsetting the effect of increase in the gas velocity.

6. Application to the Actual Production Process

Along with the expansion of application of converter type hot-metal pretreatment, Nippon Steel Corporation has promoted the de-

velopment of high-speed blowing technology to enhance productivity. Particularly, in parallel with the development of high-speed blowing, suppression of the amount of dust and spitting has become a serious subject as a means to improve molten steel yield. Therefore, Nippon Steel Corporation has conducted optimization of lance design and oxygen feeding condition (such as oxygen feeding rate, lance height) on the basis of the aforementioned findings and simulation technology. Among them, findings related to incorrect expansion and estimation technology of jet interference and coalescence behavior by CFD simulation are effectively utilized in optimizing jet intensity and dispersion, thus contributing to the prevention of deterioration in yield under high-speed blowing.[19, 20)]

7. Conclusion

Through experiments and CFD simulation, Nippon Steel Corporation has promoted elucidation of phenomena relating to a top-blowing jet, such as incorrect expansion, interference and coalescence, interaction with bath, behavior in the combustion field and the following knowledge has been obtained:

1) Central axial jet velocity of a single-hole nozzle in the state of incorrect expansion can be arranged unitarily for the most part by the extent of incorrectness, and estimation of velocity in the state of incorrect expansion has become possible. By positively employing incorrect expansion, a softly blown jet has been realized.
2) The CFD simulation result for velocity distribution of a multi-hole nozzle jet, including the behavior of interference and coalescence of the jet, substantially shows good agreement with the measurement result, and therefore it can be said that a reasonable simulation technology has been established.
3) As to the interaction of a jet with a bath, although direct simulation by CFD cannot reproduce satisfactorily, CFD simulation of jet velocity distribution has enabled the estimation of jet collision momentum and cavity shape (depth, radius), and though indirectly, the estimation of the spitting generating rate and spitting scattering height has also been made possible.
4) As to the jet behavior in a combustion field, a simulation model capable of reproducing the measured result of gas concentration distribution and temperature has been established, based on which, jet characteristics have been estimated. As a result, it was shown that dynamic pressures of a jet under combustion and the one at nonreacting room temperature are approximately equal.

Currently, Nippon Steel Corporation is conducting design and operation of a top-blowing lance of a converter utilizing above knowledge and simulation technology. However, despite the effects of gas and those generated at the spot of collision of a jet with the bath (hot spot)[21)] and the effect of slag are not matters to be ignored in nature; they are not sufficiently taken into consideration because of their complexity of phenomena. Authors are determined to further elucidate the above-mentioned subjects by incorporating sensing technologies and novel simulation models to realize further enhancement of efficiency and productivity of converter refining operation.

References

1) Segawa, K.: Tetsu Yakin Hannou Kogaku (Ferro-metallurgy Reaction Engineering). Revised New Edition. Tokyo, Nikkan Kogyo Shimbun, 1977
2) Ogawa, Y. et al.: Tetsu-to-Hagané. 87 (1), 21 (2001)
3) Hayashi, H. et al.: CAMP-ISIJ.. 15 (1), 139 (2002)
4) Naito, K. et al.: ISIJ Int. 40 (1), 23 (2000)
5) Asahara, N. et al.: CAMP-ISIJ. 23 (2), 554 (2010)
6) Asahara, N. et al.: Steel Res. Int. 82 (5), 587 (2011)
7) Fluent Inc.: FLUENT User's Guide (CD-ROM). New Hampshire, Fluent Inc., 2006
8) Ishikawa, H. et al.: Tetsu-to-Hagané. 58 (1), 76 (1972)
9) Turkdogan, E.T.: Chem. Eng. Sci. 21, 1133 (1966)
10) Tanaka, T. et al.: Tetsu-to-Hagané. 74 (8), 1953 (1988)
11) Mori, M. et al.: Tetsu-to-Hagané. 70 (4), S244 (1984)
12) Banks, R.B. et al.: J. Fluid Mech. 15 (1), 13 (1963)
13) Cheslak, F.R. et al.: J. Fluid Mech. 36 (1), 55 (1969)
14) Kaizawa, A. et al.: 8th International Conference on CFD in Oil and Gas, Metallurgical and Process Industries. Trondheim, 2011
15) Sumi, I. et al.: ISIJ Int. 46 (9), 1312 (2006)
16) Kato, Y. et al.: Tetsu-to-Hagané. 75 (3), 478 (1989)
17) Koga, T. et al.: Transactions of the Japan Society of Mechanical Engineers (Series B). 72 (723), 2798 (2006)
18) Hirai, M. et al.: Tetsu- to- Hagané. 73 (9), 1117 (1987)
19) Kumakura, M. Shinnittetsu Giho. (394), 4 (2012)
20) Hashimoto, H. et al.: Shinnittetsu Giho. (394), 84 (2012)
21) Kitamura, S. et al.: Tetsu-to-Hagané. 76 (2), 199 (1990)

Ken-ichiro NAITO
Chief Researcher
Steelmaking R&D Div.
Process Technology Center
20-1 Shintomi, Futtsu, Chiba 293-8511

Norifumi ASAHARA
Senior Researcher
Yawata R&D Lab.

Akihide KAIZAWA
Researcher
Steelmaking R&D Div.
Process Technology Center

Yuji OGAWA
Chief Researcher, Dr.Eng.
Steelmaking R&D Div.
Process Technology Center

Itsuro KITAGAWA
Manager
Technical Cooperation Dept.
Technical Administration & Planning Div.

Takeo INOMOTO
Senior Researcher
Steelmaking R&D Div.
Process Technology Center

Naoto SASAKI
Senior Researcher
Steelmaking R&D Div.
Process Technology Center

Michitaka MATSUO
General Manager, Dr.Eng.
Steelmaking R&D Div.
Process Technology Center